Available online at www.sciencedirect.com
SCIENCE DIRECT
International Journal of Heat and Mass Transfer 49 (2006) 1115–1128
International Journal of HEAT and MASS TRANSFER
www.elsevier.com/locate/ijhmt

Dynamics and shape of bubbles on heating surfaces: A simulation study

Yuming Chen *, Manfred Groll

Institute of Nuclear Technology and Energy Systems (IKE), University of Stuttgart, Pfaffenwaldring 31, 70569 Stuttgart, Germany

Received 10 November 2004; received in revised form 15 July 2005
Available online 2 November 2005

Abstract

The bubble shape on heating surfaces is simulated by numerically solving the Young–Laplace equation including a dynamic pressure term. This dynamic pressure is calculated by a correlation involving several empirical coefficients. By adjusting these coefficients, a given bubble shape can be well represented. Thus the pressure around the bubble and various forces acting on the bubble can be accurately calculated. Some calculation examples are given. The results show an important effect of dynamic forces on the bubble shape. Therefore, the assumption of spherical bubbles could lead to big errors in force evaluations.

Keywords: Bubble dynamics; Bubble shape; Boiling; Dynamic force; Pressure distribution; Simulation; Young–Laplace equation

1. Introduction

A growing bubble is dynamic in nature. The dynamics manifests itself in the bubble interface. Therefore, bubble dynamics can be studied by investigating bubble shapes. The first-hand knowledge of bubble geometric data can be measured through visualization experiments. These data provide a rough knowledge of bubble dynamics and they are useful in explaining the boiling phenomena and modeling the boiling heat transfer [1].

A simple (also rough) assessment of the relative importance of dynamic forces can be performed by using the Rayleigh–Plesset equation [2]. Johnson et al. [3] explained the different bubble shapes in terms of inertia and surface tension forces, viz., for hemispherical bubbles the inertia force is the dominant one; for spherical bubbles the surface tension force is greater than the inertia force; for oblate bubbles neither one of them is clearly dominant. However, the Rayleigh–Plesset equation is applied to a spherical bubble in an infinite domain of liquid, the unlimited use of this equation (also seen in many models and analyses) is in question [4], because a growing bubble is generally not spherical [4,5].

In a more sophisticated way, various forces acting on a bubble, such as buoyancy, surface tension, inertia, drag, contact pressure forces, etc., which cause the growth and departure of the bubble, can be evaluated based on the experimental bubble dynamics data [6–12]. This approach is of great interest in formulating the correlations for the bubble departure diameter under various conditions and in investigating the bubble detachment condition. However, the accuracy of this kind of evaluation seems to be rather poor, since most of the calculation results give a relatively big non-zero net force throughout the bubble lifetime.

Reverse to the approaches mentioned above, a bubble shape can be predicted by modeling two-phase flow around the vapor–liquid interface. A gas bubble growing on a submerged needle or orifice has been subjected to intensive investigations for several decades [4,5,13–15]. The accuracy of model predictions has been improved consistently. However, the idealizations involved in each model limit the area of applications.

Unlike a growing gas bubble, the vapor flow rate into a growing bubble on a heating wall cannot be explicitly known. The mechanisms of a bubble growing on a heating wall are extremely complicated and are greatly influenced

* Corresponding author. Fax: +49 711 6852010.
E-mail address: Chen@ike.uni-stuttgart.de (Y. Chen).

0017-9310/$ - see front matter © 2005 Elsevier Ltd. All rights reserved.
doi:10.1016/j.ijheatmasstransfer.2005.07.053

Nomenclature

a	coefficient in bubble growth law $R = at^b$ [m/s^b]
$\underline{A}$	area [m^2]
$\vec{A}$	area vector [m^2]
b	exponent in bubble growth law $R = at^b$ [–]
C_V, C_L	constants in Eqs. (1) and (2) [Pa]
C_1, C_2, C_3	coefficients in Eq. (10) [–]
C_M	added mass coefficient [–]
C_S	coefficient in Eq. (22) [–]
D	bubble diameter [m]
F	force [N]
g	acceleration of gravity [m/s^2]
$\hat{g}$	$\vec{g}/\lvert\vec{g}\rvert$, unit vector in the direction of gravity [–]
h	bubble height [m]
Ja	$\rho_L C_p \Delta T/(h_{fg}\rho v)$, Jakob number [–]
$n1, n2$	coefficients in Eq. (10) [–]
$\vec{n}$	normal vector shown in Fig. 1 [–]
P	pressure [Pa]
ΔP	Laplace pressure drop [Pa]
ΔP_D	$P_D - P_{D0}$, dynamic pressure difference [Pa]
R	bubble radius [m]
R_0	principle radius at apex [m]
R_1, R_2	principle radii at any point [m]
r_C	radius of contact area shown in Fig. 1 [m]
S	height of bubble mass center [m]
s	arc length measured from apex [m]
ΔT	wall superheat [K]
t	time [s]
u	velocity of the bubble mass center [m/s]
V	bubble volume [m^3]
w	bubble width [m]
x	horizontal coordinate shown in Fig. 1 [m]
y	vertical coordinate shown in Fig. 1 [m]
y^*	$h - y$ [m]
y^{**}	$-(h - y)$ [m]

Greek symbols

β	contact angle [deg]
θ	angle of inclination shown in Fig. 1 [deg]
ρ	density [kg/m^3]
$\Delta\rho$	$\rho_L - \rho_V$, density difference [kg/m^3]
σ	surface tension [N/m]

Subscripts

0	at apex of bubble
B	buoyancy
CD	drag
CP	contact pressure
D	dynamic
foot	bubble foot (contact area)
int	liquid–vapor interface
L	liquid
LI	liquid inertia
max	maximum
ST	surface tension
V	vapor

by the properties of fluid and wall and by working conditions. Not until recent years, complete numerical models of a single bubble growing on an isolated nucleation site have been presented [16–19]. In these models, either a constant apparent contact angle [16,17], or a truncated spherical bubble [18,19] are assumed a priori, In fact, the bubble shape can change dramatically during the growing process. A truncated spherical bubble is a poor assumption in many cases. The contact angle is dynamic during bubble growth and is different from the static contact angle. Under these assumptions, a good fit of a real bubble shape is difficult. Since the Laplace pressure drop is very sensitive to the bubble shape, a poorly simulated bubble interface indicates that, the calculated flow field is not representative of the real one.

In order to better understand boiling phenomena and eventually model boiling heat transfer, a detailed description of a single bubble behavior is the first step. The information of bubble dynamics obtained directly from experiments is not sufficient. The analyses and models generally provide idealized (or even partially wrong) information. Therefore, more efforts are needed to obtain the "real" information from real bubbles. This is the primary motivation of this study.

The idea arises from the fact that a sessile bubble or a pendent drop in the gravity field can be completely described by the Young–Laplace equation [20,21], and that a slowly growing bubble can also be simulated by the same equation with good accuracy [22], Therefore, if a dynamic bubble contour cannot be described by the Young–Laplace equation, the dynamic effects are responsible for the difference. Thus a dynamic pressure term is assumed and added into the Young–Laplace equation, so that the calculated bubble contour exactly matches the real one. This is a new approach to study bubble dynamics and to provide the necessary information for comparing with model predictions.

2. Model and numerical method

2.1. Young–Laplace equation

Fig. 1 shows schematically a bubble growing on a surface heated from below. It is assumed that the bubble is axisymmetric and the physical properties are constant, especially, no surface tension gradient exists along the interface. Therefore the Marangoni effect will not be considered. Also the tangential stress components on the inter-

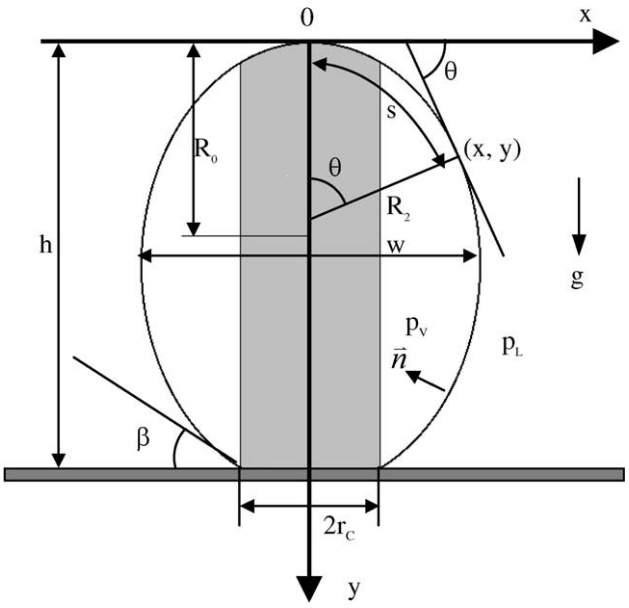

Fig. 1. A bubble growing on a heating surface.

face are neglected. The vapor and liquid pressures on the sides of the bubble interface are given by

$$P_V = \rho_V g y + P_{DV} + C_V \quad (1)$$

$$P_L = \rho_L g y + P_{DL} + C_L \quad (2)$$

where P_{DV} and P_{DL} are the dynamic pressure of vapor and liquid, respectively, which can be induced by inertia, drag, vapor momentum, etc.; C_V and C_L, are constants taken as references for hydrostatic pressures. The pressure variation across the liquid–vapor interface is described by the Young–Laplace equation, using Eqs. (1) and (2), as

$$P_V - P_L = (\rho_V - \rho_L) g y - P_D + (C_V - C_L) = \sigma\left(\frac{1}{R_1} + \frac{1}{R_2}\right) \quad (3)$$

where $P_D = P_{DL} - P_{DV}$. R_1 and R_2 are local principle radii of curvature. At $y = 0$: $R_1 = R_2 = R_0$ and $P_D = P_{D0}$, the dynamic pressure difference at the apex. Then from Eq. (3):

$$C_V - C_L = \frac{2\sigma}{R_0} + P_{D0} \quad (4)$$

By using Eq. (4), Eq. (3) is changed to

$$\Delta P = P_V - P_L = \sigma\left(\frac{1}{R_1} + \frac{1}{R_2}\right) = \frac{2\sigma}{R_0} - \Delta\rho g y - \Delta P_D \quad (5)$$

with $\Delta\rho = \rho_L - \rho_V$ and $\Delta P_D = P_D - P_{D0}$, the dynamic pressure difference in respect to the apex. ΔP is the Laplace pressure drop, $\Delta\rho g y$ is the hydrostatic pressure difference.

2.2. Numerical method

Using differential geometric relations, Eq. (5) can be rewritten as:

$$\Delta P = \sigma\left(\frac{d\theta}{ds} + \frac{\sin\theta}{x}\right) = \frac{2\sigma}{R_0} - \Delta\rho g y - \Delta P_D \quad (6)$$

$$\frac{dx}{ds} = \cos\theta \quad (7)$$

$$\frac{dy}{ds} = \sin\theta \quad (8)$$

where θ is the inclination at any point (x, y) and s is the length measured from the apex (Fig. 1). This is a system of first-order differential equations which can be solved numerically with the boundary condition given by

$$x = y = 0; \quad \theta = 0 \quad (9)$$

The Laplace pressure drop ΔP is expressed empirically as

$$\Delta P = \left\{1 + C_1 \sin\left[2\pi\left(1 - \left(\frac{y}{h}\right)^{n1}\right)\right]\right\} \times \left\{\frac{2\sigma}{R_0} - \Delta\rho g y\left[C_2 - C_3\left(\frac{y}{h}\right)^{n2}\right]\right\} \quad (10)$$

where h is the bubble height; C_b C_2, C_3, $n1$ and $n2$ are coefficients which are used to adjust the calculated bubble shape to fit the real one. Eq. (10) is not formulated based on fundamental physics (which we think cannot lead to an accurate simulation of bubble shapes in many cases), rather it is mainly based on numerical tests. The basic idea behind Eq. (10) is that, the dynamic pressure difference ΔP_D is a function of position (y/h). The value of ΔP_D can be related to that of the hydrostatic pressure. The first term on the r.h.s. of Eq. (10) is mainly used to adjust the curvature and the height of the mass center, the second term is mainly used to adjust the diameter of the bubble base and the curvature at the neck area. Eq. (10) may not be the best possible correlation, but it enables us to simulate bubbles of various shapes rather well.

A real bubble is simulated in a heuristic way. First the bubble height h and bubble width w are used in the computer program. The coefficients in Eq. (10) are set without considering the dynamic effects ($C_1 = C_3 = 0$, $C_2 = 1$, i.e. $\Delta P_D = 0$). Before the calculation, the principle radius at the apex R_0 is assumed. Then Eqs. (6)–(10) are solved by a fourth-order Runge–Kutta routine point by point with increasing the arc length s by steps Δs until x reaches the maximum x_{max}. If x_{max} is not equal to half of the real bubble width $(w/2)$, R_0 is changed and the procedure is repeated. Otherwise, the program goes on to the next step until y equal the real bubble height h. Then the calculated bubble contour is compared to the real one. If it does not fit the real bubble contour, the coefficients in Eq. (10) are changed and the calculation procedure is repeated until a satisfying result is achieved. There is no numerical contour criterion, but a visual comparison is made between calculated and observed contours.

From this calculation, the distributions of Laplace pressure drop (ΔP) and hydrostatic pressure ($\Delta\rho g y$) are obtained. The absolute dynamic pressure is not available, while the dynamic pressure difference (ΔP_D) can be calculated from Eq. (5).

2.3. Forces acting on a bubble

The integration of Eq. (5) over the liquid–vapor interface area (int) considering only the vertical direction, gives

$$\int_{\text{int}} \Delta P \,\mathrm{d}\vec{A}\cdot\hat{g} = \int_{\text{int}} \frac{2\sigma}{R_0}\mathrm{d}\vec{A}\cdot\hat{g} - \int_{\text{int}} \Delta\rho g y \,\mathrm{d}\vec{A}\cdot\hat{g} - \int_{\text{int}} (P_{\text{D}} - P_{\text{D0}})\,\mathrm{d}\vec{A}\cdot\hat{g} \tag{11}$$

where, $\mathrm{d}\vec{A} = \vec{n}\,\mathrm{d}A$ with the normal vector $\vec{n}$ taken inward, and $\hat{g} = A/|\vec{g}|$ is the unit vector in the direction of gravity. Considering that the vapor phase is enclosed by the liquid–vapor interface area and the bubble foot area (foot), Eq. (11) changes to

$$\int_{\text{int}} \Delta P\,\vec{n}\cdot\hat{g}\,\mathrm{d}A - \int_{\text{int+foot}} \frac{2\sigma}{R_0}\vec{n}\cdot\hat{g}\,\mathrm{d}A + \int_{\text{foot}} \frac{2\sigma}{R_0}\vec{n}\cdot\hat{g}\,\mathrm{d}A + \int_{\text{int+foot}} \Delta\rho g y\,\vec{n}\cdot\hat{g}\,\mathrm{d}A - \int_{\text{foot}} \Delta\rho g y\,\vec{n}\cdot\hat{g}\,\mathrm{d}A + \int_{\text{int}} P_{\text{D}}\,\vec{n}\cdot\hat{g}\,\mathrm{d}A - \int_{\text{int+foot}} P_{\text{D}}\,\vec{n}\cdot\hat{g}\,\mathrm{d}A + \int_{\text{foot}} P_{\text{D}}\,\vec{n}\cdot\hat{g}\,\mathrm{d}A = 0 \tag{12}$$

Combining the three terms involving integration over the foot area, viz. the third, the fifth and the last term, and using Eqs. (1), (2) and (4), gives

$$\int_{\text{foot}} \left(\frac{2\sigma}{R_0} - \Delta\rho g y + P_{\text{D0}}\right)\vec{n}\cdot\hat{g}\,\mathrm{d}A = \int_{\text{foot}} \Delta P|_{y=h}\,\vec{n}\cdot\hat{g}\,\mathrm{d}A + \int_{\text{foot}} P_{\text{D}}|_{y=h}\,\vec{n}\cdot\hat{g}\,\mathrm{d}A \tag{13}$$

Here $\Delta P|_{y=h}$ and $P_{\text{D}}|_{y=h}$ are the Laplace pressure drop and the dynamic pressure difference at the triple contact line. Combining Eqs. (12) and (13) and noting that the second and the seventh terms in Eq. (12) equal zero, Eq. (12) changes to

$$\int_{\text{int}} \Delta P\,\vec{n}\cdot\hat{g}\,\mathrm{d}A + \int_{\text{int+foot}} \Delta\rho g y\,\vec{n}\cdot\hat{g}\,\mathrm{d}A + \left(\int_{\text{int}} P_{\text{D}}\,\vec{n}\cdot\hat{g}\mathrm{d}A + \int_{\text{foot}} P_{\text{D}}|_{y=h}\,\vec{n}\cdot\hat{g}\,\mathrm{d}A\right) + \int_{\text{foot}} \Delta P|_{y=h}\,\vec{n}\cdot\hat{g}\,\mathrm{d}A = 0 \tag{14}$$

The first term in Eq. (14) is the surface tension force (F_{ST}) in the direction of $\hat{g}$ which can be changed into an alternative form by using Eqs. (6) and (7):

$$F_{\text{ST}} = \int_{\text{int}} \Delta P\,\vec{n}\cdot\hat{g}\,\mathrm{d}A = 2\pi\sigma r_{\text{C}}\sin\beta \tag{15}$$

where r_{C} is the radius of the contact area and β is the contact angle. The second term in Eq. (14) is the buoyancy force (F_{B}) in the direction of $\hat{g}$:

$$F_{\text{B}} = \int_{\text{int+foot}} \Delta\rho g y\,\vec{n}\cdot\hat{g}\,\mathrm{d}A = -\Delta\rho g V \tag{16}$$

The third term in Eq. (14) is the dynamic force (F_{D}):

$$F_{\text{D}} = \int_{\text{int}} P_{\text{D}}\,\vec{n}\cdot\hat{g}\,\mathrm{d}A + \int_{\text{foot}} P_{\text{D}}|_{y=h}\,\vec{n}\cdot\hat{g}\,\mathrm{d}A = \int_{\text{int}} P_{\text{D}}\,\vec{n}\cdot\hat{g}\,\mathrm{d}A + \pi r_{\text{C}}^2 P_{\text{D}}|_{y=h} \tag{17}$$

which can be positive or negative. This force is the sum of liquid and vapor inertia, drag and vapor momentum forces, etc. The last term in Eq. (14) is the contact pressure force (F_{CP}) and it can be changed to

$$F_{\text{CP}} = \int_{\text{foot}} \Delta P|_{y=h}\,\vec{n}\cdot\hat{g}\,\mathrm{d}A = -\pi r_{\text{C}}^2 \Delta P|_{y=h} \tag{18}$$

which is generally in the direction of $-\hat{g}$. This contact pressure force is due to the pressure difference inside and outside of the bubble interface at the triple (contact) line and acts over an area of the size of the contact area. It can also be interpreted as a reaction force acting on the bubble [23].

This force was also called the "corrected buoyancy force" [24],[1] A similar procedure for deducing F_{CP} was also given in [6].

According to Eq. (14), the total force acting on the bubble equates zero, viz.

$$\sum F = F_{\text{ST}} + F_{\text{CP}} + F_{\text{B}} + F_{\text{D}} = 0 \tag{19}$$

After the simulation of a bubble, the forces acting on it can also be calculated. Conventionally, the force which acts in assisting the bubble detachment is taken as positive force, i.e. acting in the negative y-direction.

3. Simulation examples

3.1. Bubbles growing on an enhanced tube

Enhanced surfaces have been widely used in industry. Fig. 2 shows the cut-view of surface pores and sub-surface channels of an enhanced tube (19.05 mm outer diameter; for experimental set-up refer [25]). The growth of bubbles on this kind of enhanced surfaces is mainly attributed to the inflow of vapor from the sub-surface channels [1,25]. This is similar to the gas bubbles growing from submerged orifices connected to a gas chamber. Compared to the bubbles growing on the smooth surfaces, the bubbles are more dynamics-controlled for the enhanced surfaces [25]. It is therefore of interest to study this kind of bubbles.

[1] Eq. (16) for the buoyancy force implies that the vapor pressure is equal to the hydrostatic liquid pressure at the plane of the bubble base. Therefore, a corrected force arises which is included in Eq. (18). But when the dynamic forces cannot be neglected, this term actually also includes the effects of dynamic force, therefore it is the "corrected buoyancy and dynamic force".

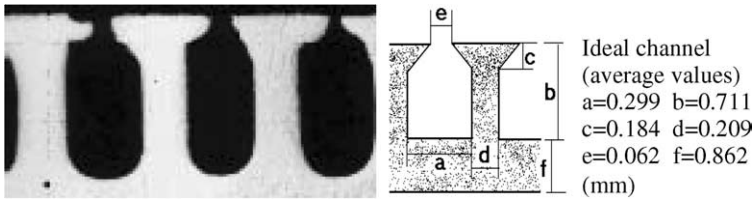

Fig. 2. Surface pores and sub-surface channel geometry for enhanced surface.

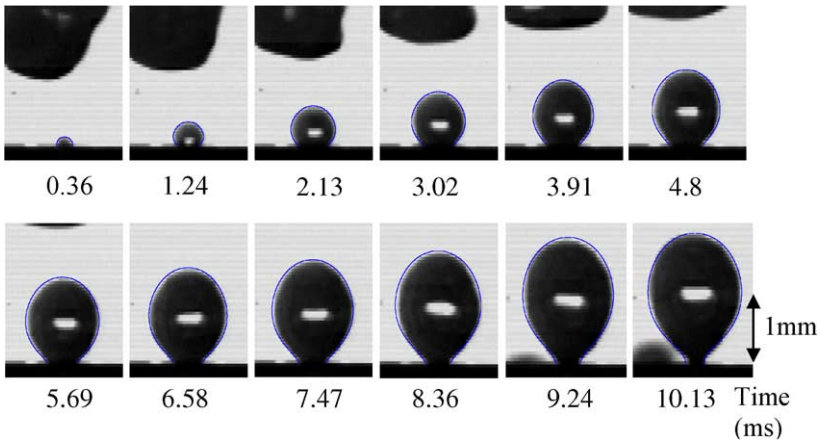

Fig. 3. A bubble growing on enhanced surface (isobutane, $T_S = 283$ K, $P_S = 2.17$ bar, $q = 2$ kW/m^2).

Two typical contours of bubbles growing on the top surface' of the enhanced tube with isobutane and propane as working fluids are shown in Figs. 3 and 4, respectively. The bubble interface including the neck region can be described by Eq. (10). A better simulation requires a higher resolution of the video pictures. For low resolutions, such as for the small bubbles at the initial growth stage, a comparison between the simulated and the experimental bubble shapes is difficult.

Fig. 5a–d show the distribution of the hydrostatic pressure ($\Delta\rho gy$, left side of bubble contour) and dynamic pressure difference (ΔP_D, right side of bubble contour) around the bubble.[2] $\Delta\rho gy$ increases continuously from the bubble top to the bubble base and is much smaller than ΔP_D especially for bubbles with higher aspect ratio (h/w). In most cases, ΔP_D is in the same direction as $\Delta\rho gy$. However, ΔP_D can be negative or positive.[3] Negative ΔP_D is found at the lower part of the bubble at the initial growth stage (Fig. 5a) and, more significantly, at the necking stage (Fig. 5d). In both cases, the accelerating growth or rise of the bubble induces a low liquid pressure area at the lower part of the bubble.

Fig. 6a and b shows the calculated forces acting on the growing bubbles shown in Figs. 3 and 4 by using the method described in Section 2.3. During most of the bubble lifetime, the only negative force (resisting detachment) is the surface tension force which tends to zero when approaching bubble detachment. The buoyancy force is important at the later growth stage while the contact pressure force is important at the early growth stage. Immediately after the bubble is initiated, the dynamic force is negative for a very short time period which means the ambient liquid tends to resist the rapid expansion of the initial bubble (only shown in Fig. 6a where a better quality of video pictures of small initial bubbles is available). Then the dynamic force turns gradually positive (pulling force) and the bubble shows an elongated shape. This pulling force first increases then decreases as the bubble keeps growing. Finally it turns negative again when the bubble undergoes the necking process and begins an accelerating rise from the surface.

3.2. Bubbles growing on smooth planar surfaces

3.2.1. Moderate Jakob number

Fig. 7 shows the pictures of bubbles taken by Han and Griffith [26]. The bubbles were generated on a horizontal gold surface polished by No. 8 diamond compound with degassed distilled water as working fluid. The Jakob number Ja is 48.7. The bubble shows a hemispherical or oblate shape at the early growth stage then it changes to an elongated shape as it is proceeding towards detachment. Five bubble contours (at times t1–t5) of this growth sequence

[2] The lines of pressure vectors in the figures are not evenly distributed around the bubble contours. This is because the vectors were drawn for given inclination angles with a constant interval. Therefore, at the place where the inclination angle has little change, there is a bigger interval between neighboring vector lines.

[3] The positive hydrostatic pressure and dynamic pressure differences counteract the expansion of the liquid–vapor interface, and are positive in the direction from the liquid side to the vapor side.

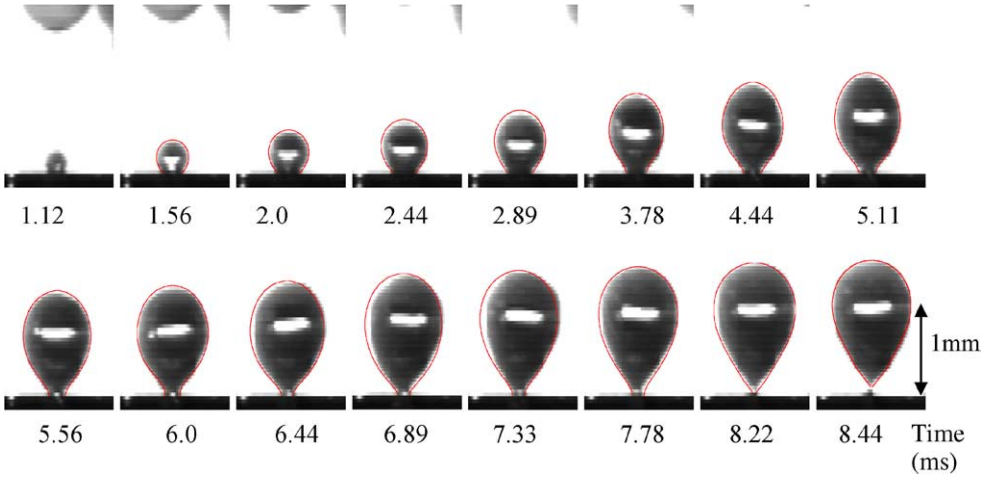

Fig. 4. A bubble growing on enhanced surface (propane, $T_S = 293$ K, $P_S = 8.36$ bar, $q = 6.5$ kW/m^2).

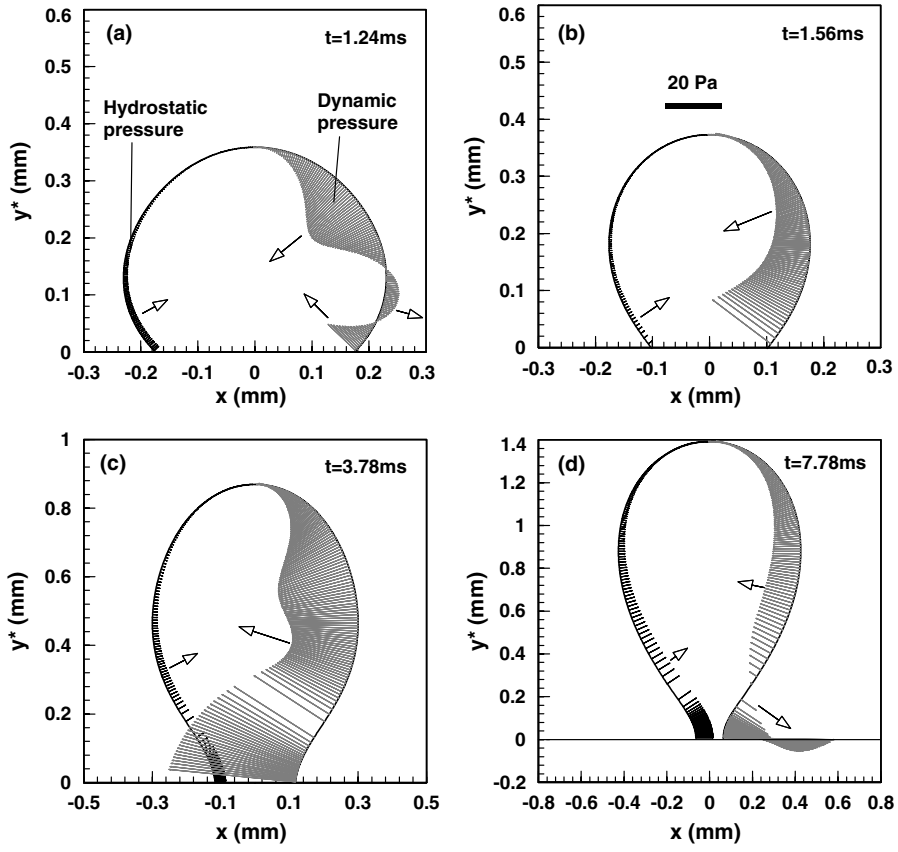

Fig. 5. Distributions of hydrostatic and dynamic pressure around bubbles on enhanced surface ($y^* = h - y$). (a) Isobutane, $T_S = 283$ K, $P_S = 2.17$ bar, $q = 2$ kW/m^2. (b)–(d) Propane, $T_S = 293$ K, $P_S = 8.36$ bar, $q = 6.5$ kW/m^2.

have been simulated and the calculated bubble contours are also shown in Fig. 7.

The distribution of the pressure differences, $\Delta\rho gy$ and ΔP_D, around the bubble is shown in Fig. 8. In general, ΔP_D is greater than $\Delta\rho gy$ at the early growth stage, while it is much less than $\Delta\rho gy$ at the later growth stage. This is quite different from the distributions shown in Fig. 5 for the enhanced surface, although the evolution of the bubble shapes is similar for both cases. Fig. 9 shows the forces acting on the bubble. The dynamic force acts to hold the bubble on the wall at the early growth stage, then it pulls the bubble to an elongated shape when the bubble growth rate slows down, and finally it turns negative again to counteract the accelerating rise of the bubble at the

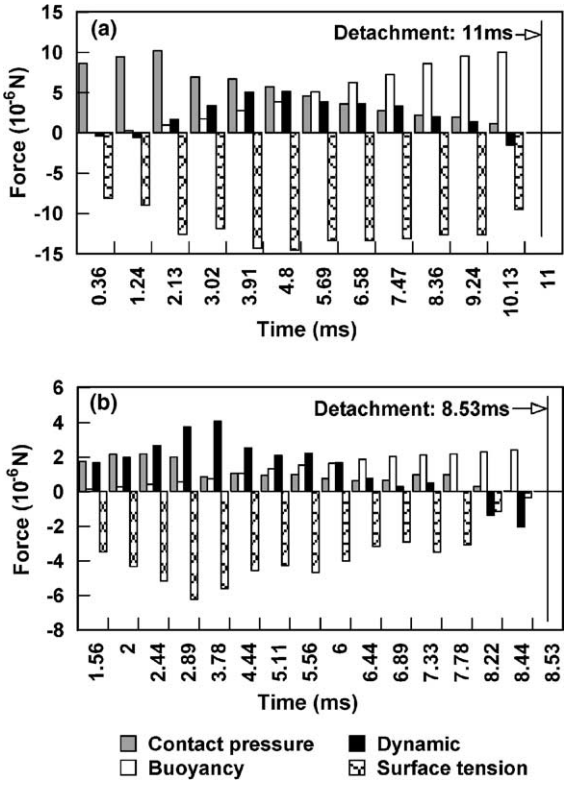

Fig. 6. Forces acting on a growing bubble on enhanced surface. (a) Isobutane, $T_S = 283$ K, $P_S = 2.17$ bar, $q = 2$ kW/m^2. (b) Propane, $T_S = 293$ K, $P_S = 8.36$ bar, $q = 6.5$ kW/m^2.

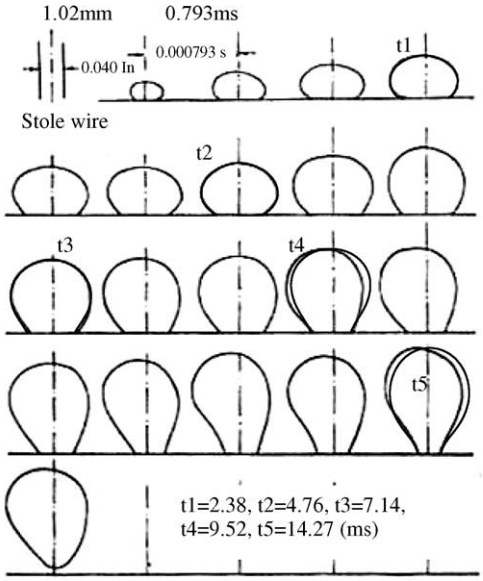

Fig. 7. Bubble growing on a smooth plane surface [26] (water, $T_S = 359$ K, $P_S = 0.597$ bar, $\Delta T_W = 10$ K, $Ja = 48.7$).

necking stage. The magnitudes of the dynamic pressure difference (Fig. 8) and the dynamic force (Fig. 9) indicate that the bubble is more dynamics-controlled at the early growth stage than at the later stage as it is quite well known for bubbles growing on smooth surfaces [27].

3.2.2. Relatively high Jakob number

Fig. 10 shows the pictures of bubbles taken by Van Stralen et al. [27] under relatively high Jakob number ($Ja = 108$). The bubbles were generated on a cylindrical artificial nucleation cavity (diameter: 25 μm, depth: 100 μm) on the top face of a horizontal nickel-plated copper rod with surface roughness within 0.2 μm. Water is used as working fluid. Four calculated bubble contours (at times t1–t4) are also shown in Fig. 10. Although the upper part of the bubble just before detachment (at t4) can be well simulated, the lower part cannot be simulated by using Eq. (10) due to the very sharp change of the curvature near the middle point of the bubble contour (indicated by a solid arrow in Figs. 10 and 11). Thus the values of (x, y) on the lower bubble contour are directly taken from the picture and then fitted by a sixth-order polynomial equation which is then used to calculate the pressure differences.

Fig. 11 shows the distribution of pressure differences around the bubble (the jump of ΔP_D at the middle part of the bubble at t4 is due to the non-smooth joint of the two calculations for the upper and lower parts of the bubble contour, as mentioned above). In general, $\Delta\rho gy$ and ΔP_D have a similar magnitude, but act in different directions. Just before detachment (at time t4), the Laplace pressure drop is negative at the lower part of the interface which means the liquid pressure is higher than the vapor pressure, especially near the contact area where the absolute value of ΔP_D is small.[4]

Fig. 12 shows the forces acting on the growing bubble. The dynamic force is found important throughout the bubble lifetime and acts in such a way that the bubble is kept in a hemispherical or an oblate shape.

4. Discussions

4.1. Dynamic effects

The simulation results show an important role of dynamic effects on a growing bubble. This can be demonstrated by comparing simulated bubble shapes with and without considering the dynamic pressure term as shown in Fig. 13a and b. In Fig. 13a, for a (relatively big) spherical bubble growing on the bottom surface of the enhanced tube, if the dynamic effects are not considered, and if the observed bubble width and bubble base diameter are taken, then the simulated bubble height would be smaller than the observed one, namely, the bubble would actually show an oblate shape due to the upward buoyancy force. Therefore, for this relatively big spherical bubble, the surface tension force does not necessarily dominate as stated in [3],

[4] It is possible that there is a neck formed at the very small area of the bubble base. In this case, $1/R_1$ is a very large positive value, and $1/R_2$ is a small negative value. As a result, the Laplace pressure drop would be a very big positive value in this small neck area which, according to [28], is responsible for the liquid jet observed in [27,28].

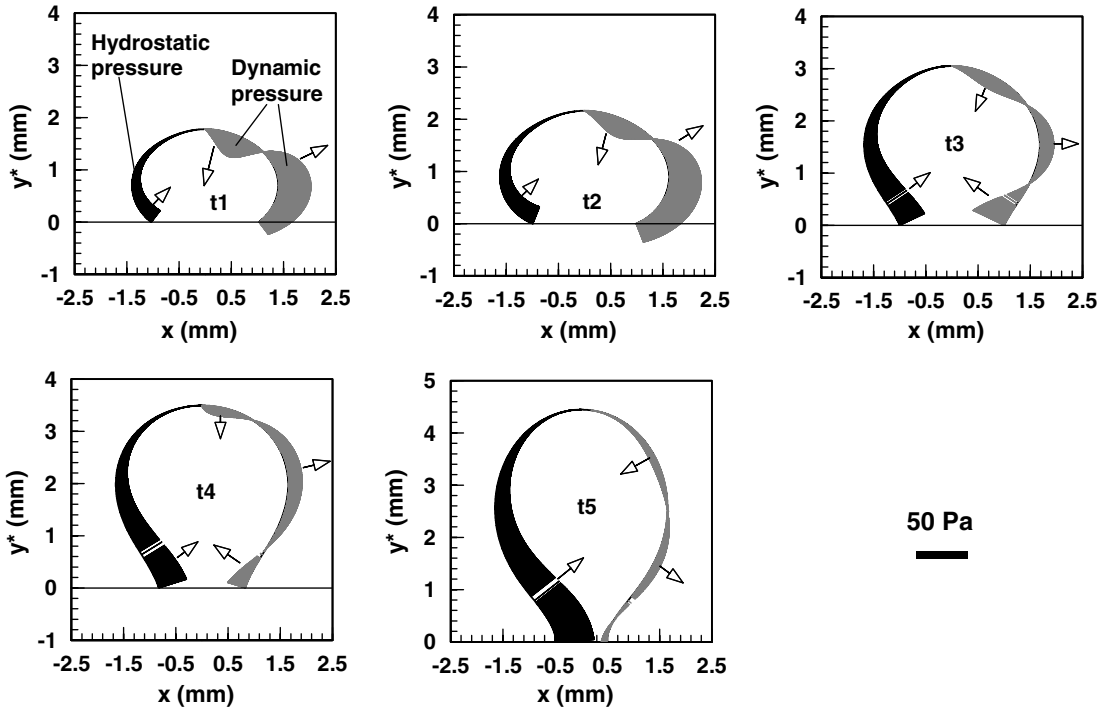

Fig. 8. Distributions of hydrostatic and dynamic pressure for bubble shown in Fig. 7 (water, $T_S = 359$ K, $P_S = 0.597$ bar, $\Delta T_W = 10$ K, $Ja = 48.7$).

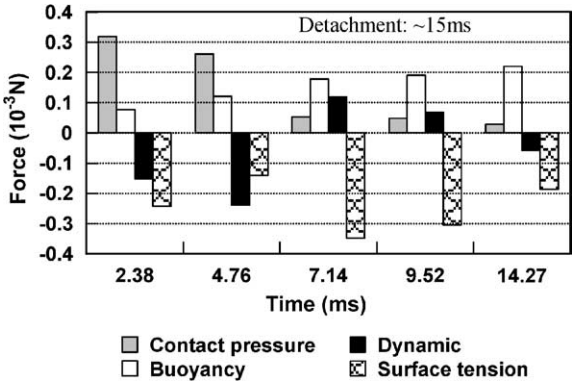

Fig. 9. Forces acting on the growing bubble shown in Fig. 7 (water, $T_S = 359$ K, $P_S = 0.597$ bar, $\Delta T_W = 10$ K, $Ja = 48.7$).

However, for a small spherical bubble, where the surface tension force is dominant, the bubble shape can be well simulated without considering the dynamic effects (not shown). For an elongated bubble, as the one shown in Fig. 7 at time t5, if the dynamic effects are not considered, the simulated bubble does show an elongated shape due to the upward buoyancy force, but it has a much bigger contact area than the real one (the bubble height and bubble width are kept the same) (Fig. 13b).

4.2. Bubble shapes and dynamics

Johnson et al. [3] classified three kinds of bubble shapes, viz., spherical, hemispherical and oblate bubbles. Besides these three kinds of bubble shapes, the elongated bubble is another important bubble shape for boiling on heating walls. Fig. 14 shows the evolution of bubble shapes during growth in terms of aspect ratio (here defined as h/w) against dimensionless growth time (t/t_d). Since there is a contact area between the bubble and the wall, a seemingly spherical bubble does not have an aspect ratio of unity. A bubble which detaches in an oblate shape shows initially a hemi-

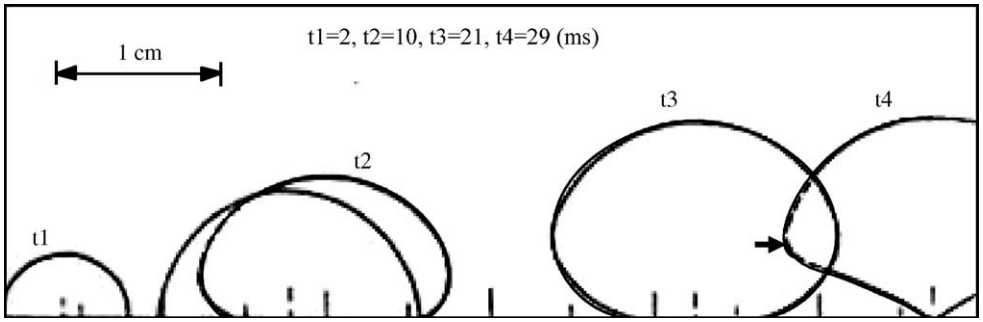

Fig. 10. Bubble growing on a smooth surface (top side of a rod) [27] (water, $T_S = 339.6$ K, $P_S = 0.267$ bar, $\Delta T_W = 14.6$ K, $q = 53.2$ kW/m^2, $Ja = 108$).

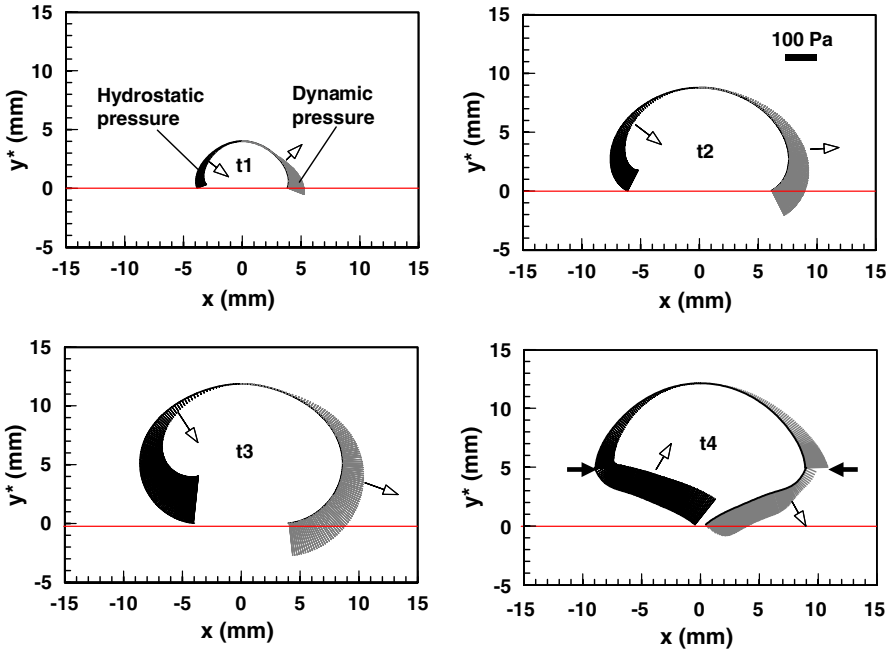

Fig. 11. Distributions of hydrostatic and dynamic pressure for bubble shown in Fig. 10 (water, $T_S = 339.6$ K, $P_S = 0.267$ bar, $\Delta T_W = 14.6$ K, $q = 53.2$ kW/m^2, $Ja = 108$).

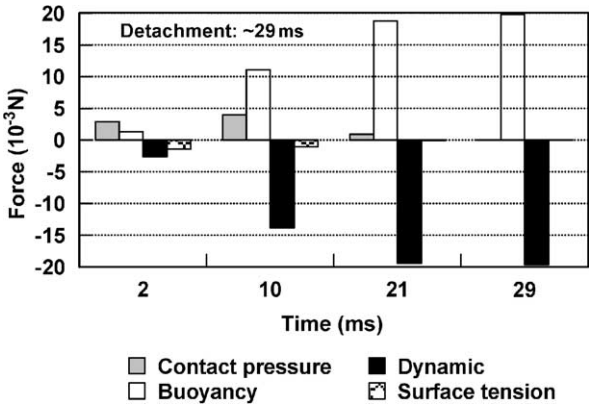

Fig. 12. Forces acting on the growing bubble shown in Fig. 10 (water, $T_S = 339.6$ K, $P_S = 0.267$ bar, $\Delta T_W = 14.6$ K, $q = 53.2$ kW/m^2, $Ja = 108$).

spherical shape and then changes to an oblate shape. A bubble which detaches in a relatively spherical shape shows initially a hemispherical or oblate shape for a very short period, then it changes to a spherical shape [25]. A bubble which detaches in an elongated shape changes from a hemispherical shape at the very beginning to an oblate, spherical, then to an elongated shape and, finally a neck is formed, which generally can be clearly seen, and then the bubble breaks away.

A pattern (shape) map of bubbles can be possibly developed by relating the aspect ratio (h/w) to the ratio of dynamic and buoyancy forces F_D/F_B, Fig. 15a. The relationship between F_D/F_B and dimensionless growth time (t/t_d) is shown in Fig. 15b. The results can be summarized as follows:

- Both *hemispherical* $h/w < \sim 0.7$) *and oblate bubbles* ($\sim 0.7 < h/w < \sim 0.9$) occur at $F_D/F_B < -1$, which means that the dynamic force resists the expansion of the bubble and is more important than the buoyancy force, especially at the early growth stage (Fig. 15b), the (liquid) inertia-controlled stage [27]. For the water vapor bubble shown in Fig. 15 for $Ja = 108$, the liquid inertia force is important throughout the whole growth period. This is a kind of so-called "Rayleigh" bubble [27]. The negative dynamic pressure difference ΔP_D is big at the lower part of the bubble interface (Fig. 11). This local depression was thought to be partially responsible for the rapid generation of a secondary vapor column or bubble right after the departure of a "Rayleigh" bubble [27,29].
- For *elongated bubbles* ($h/w > \sim 0.9$), F_D/F_B is generally positive (except during the necking period); which means that the dynamic force acts in the same direction as buoyancy force. For the bubbles growing on the enhanced tube (at relatively high pressure), F_D/F_B can be much higher than unity for $h/w < 1.1$. In this case, the vapor momentum force plays an important role. For example, for the bubble shown in Fig. 4 at time 7.78 ms, the vapor velocity through the surface pore (about 0.2 mm in diameter) is about 2.5 m/s which induces a maximum pressure on the interface of about 56 Pa ($1/2\rho_v u_v^2$),[5] while the hydrostatic pressure difference is less than

[5] For a bubble growing on a smooth surface, the vapor momentum force is generally negligible. For example, for the bubble shown in Fig. 10 at time t1, the maximum pressure on the interface induced by vapor momentum is 0.15 Pa, which is very small compared with the other pressure terms (Fig. 11). Therefore, for bubbles growing on smooth surfaces, the vapor momentum force is generally not considered.

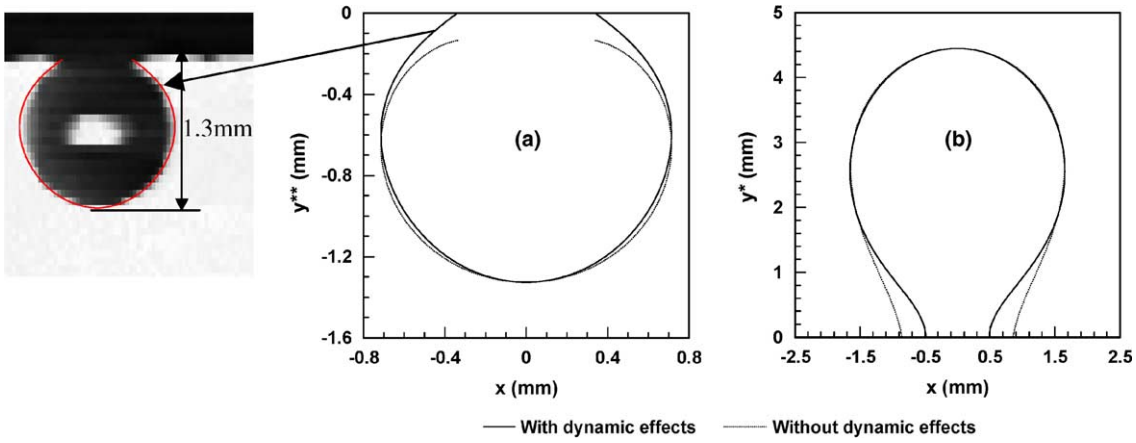

Fig. 13. Comparison of simulated bubble shapes with and without considering dynamic effects. (a) Bubble growing on the bottom surface of enhanced tube (propane, $T_S = 283$ K, $q = 9$ kW/m^2; $y^{**} = y - h$). (b) Bubble growing on a smooth surface (at the time t5 in Fig. 8).

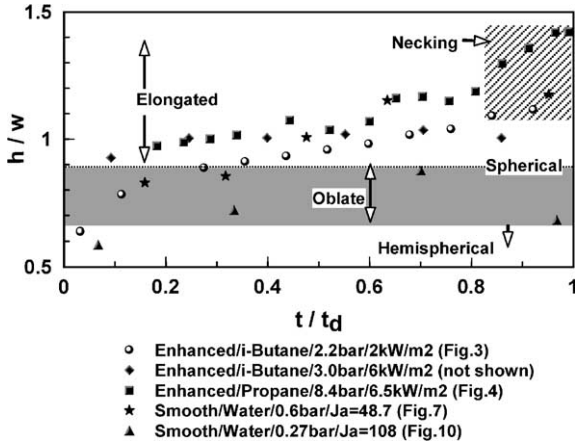

Fig. 14. Evolution of bubble shapes during growth.

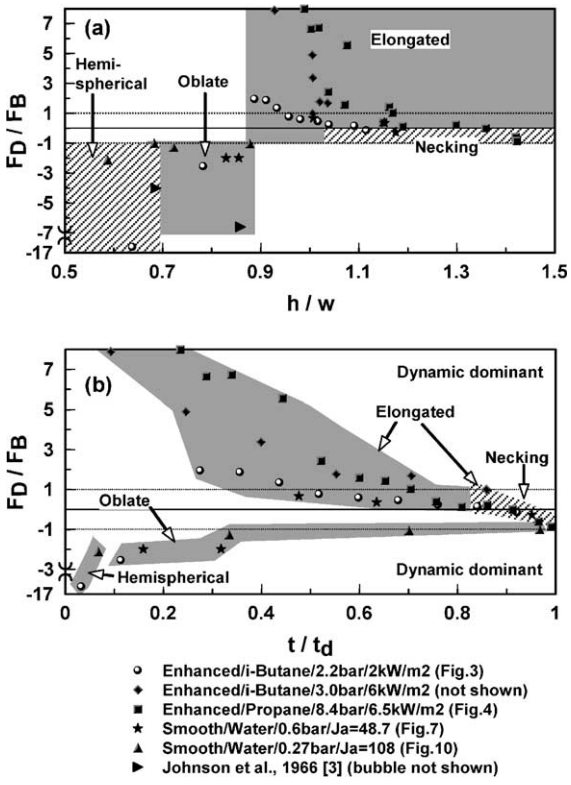

Fig. 15. (a) The ratio of dynamic and buoyancy forces against aspect ratio; (b) the ratio of dynamic and buoyancy forces against dimensionless growth time.

10 Pa (Fig. 5d). The actual vapor velocity on the interface might be much lower due to the velocity decay [15]. The effects of vapor momentum on (elongated) bubble shapes have also been demonstrated for gas bubbles growing from a submerged orifice, at least for relatively high pressure [13,15]. However, the liquid inertia force can also act in the same direction as the buoyancy force to pull the bubble to an elongated shape. This can be seen from the data for the bubble growing on the smooth surface at $Ja = 48.7$ (Fig. 15), the positive dynamic force (F_D) is attributed to the liquid inertia force, since in this case the vapor momentum and the viscous drag can be neglected.

- During the *necking period*, although the bubble still shows an elongated shape, F_D/F_B lies between 0 and -1 (Fig. 15). The negative dynamic force arises from the big negative ΔP_D at the lower part of the bubble (e.g. Fig. 5d). This low local pressure of the bubble base is induced by the accelerating rise of the bubble. A simple potential flow theory presented in [29] also shows that, as a sphere accelerates from rest on a horizontal wall, at the point at which the sphere was originally resting, the pressure suffers a sharp decrease below the ambient. Thus, for elongated bubbles, the point where the dynamic force changes from positive to negative can serve as a criterion for bubble departure (Fig. 15b).

When the data are plotted as F_P/F_{ST} against h/w, no simple relationship can be found. Thus, the explanation of different bubble shapes in terms of relative importance of

inertia and surface tension forces [3] is not supported by the present study. Note that the forces calculated in the present study are in the vertical direction. The surface tension force is actually the local force on the contact line which cannot be related to bubble size directly, rather, it is strongly influenced by the contact area and contact angle. Since the deformation of a bubble is greatly related to its size, therefore, the buoyancy force, which represents the size of a bubble, can be used to form a dimensionless group (e.g. F_D/F_B) to represent such a deformation. In fact, the forces acting on a bubble are generally evaluated by assuming spherical bubbles (such as using the Rayleigh–Plesset equation [2]) or using an equivalent diameter. The use of this method for determining the relative importance of various forces on the bubble shapes is dubious as it has been pointed out in [4].

4.3. Spherical assumption and force evaluations

Traditionally, the various forces acting on a growing bubble on a heating wall are evaluated by using theoretical or semi-theoretical equations based on the assumption of spherical bubbles [2–5,9–11]. Experimentally, the assumption of spherical bubbles or spherical bubble segments is necessary when some bubble geometric parameters are unable or difficult to be obtained by direct measurement, such as the radius of curvature which is needed for calculating the contact pressure force. In this case, an equivalent diameter based on the measured bubble volume is generally used. Theoretically, for evaluating the hydrodynamic forces, the assumption of spherical bubbles is unavoidable according to Buyevich and Webbon [30], since analytical expressions for the case of an arbitrary bubble interface represent an insurmountable task [30]. Even for a spherical segment, formidable hydrodynamic problems would arise as noted in [30] (refer also [31]).

In fact, a growing bubble on a heating wall is generally non-spherical in shape. In this case, while the spherical bubble assumption does not influence the buoyancy force, it directly leads to inaccurate evaluation of the contact pressure and surface tension forces which are generally important for a sessile bubble. Furthermore, the hydrodynamic forces could be also greatly influenced by this assumption, since these forces depend very much on the bubble shape [32]. This is clear because the local radial velocities of the bubble interface, which define the evolution of the bubble shape, strongly affect the added mass force, the viscous drag force and the gas momentum force [4,33]. For nucleate boiling on a plane wall, the gas momentum force and the drag force can generally be neglected [10,31,34]. Thus the dynamic force defined in this paper comprises essentially the added mass force. The impact of the spherical bubble assumption on the evaluation of this force will be further discussed.

For an expanding bubble moving in an otherwise quiescent liquid, the added mass force or the inertia force of the entrained liquid, F_{LI}, can be given by [35].

$$F_{LI} = -\frac{d(C_M \rho_L V u)}{dt} \tag{20}$$

here, V is the bubble volume, C_M is the added mass coefficient and u is the velocity of the bubble mass center. The shape dependency of F_{LI} can be seen by the values of C_M. For example, based on the potential flow calculations, the added mass tensor for a sphere in an unbound fluid is quite different from the two diagonal added mass tensors for an ellipsoid [36]. Rehm [11] referred C_M as a shape factor. For a growing spherical bubble tangent to a plane wall, u can be given as dR/dt, C_M is generally taken as 11/16 (for the motion of a sphere with a plane wall present [36]). Further assuming that the bubble growth law follows the form $R = at^b$ (for boiling on heating walls), then Eq. (20) changes to

$$\begin{aligned} F_{LI} &= -\frac{4}{3}\pi C_M \rho_L R^2 \left[R\frac{d^2R}{dt^2} + 3\left(\frac{dR}{dt}\right) \right] \\ &= -\frac{11}{12}\pi \rho_L a^4 b(4b-1)t^{4b-2} \end{aligned} \tag{21}$$

Eq. (21) shows that, throughout the whole growth period, F_{LI} can be either positive or negative, depending on the value of the exponent b. However, following the discussions in Section 4.2, the liquid inertia force for a bubble detached in an elongated shape can change its sign throughout the growth period (refer Fig. 9). It is also noted by Witze et al. [37] that the momentum imparted to the liquid while the bubble is growing rapidly will tend to pull the bubble from the wall after growth has slowed down. This means that the exponent b is not constant throughout the growth period, rather it is generally higher at the initial stage than at the later stage. For example, the experimental results for propane bubbles growing on a smooth tube show that b ranges from 0.61 to 0.75 for the initially inertia-controlled stage, and for the diffusion-controlled stage it ranges from 0.23 to 0.42 [25]. The direct applications of Eq. (21) are frequently seen in the literature, e.g. [12]. However, when the bubble volume and the height of mass center are fitted from measured data and using Eq. (20), the calculated F_{LI} can change its sign during the growth period [10,11]. The above discussion also confirms that the liquid inertia force is very sensitive to the bubble geometric parameters, viz. the bubble shape.

Equations with a similar form as Eq. (21) can be found in the literature [7,8,37,38]. Based on the formulation for a hemispherical bubble expanding in an inviscid liquid [6], Zeng et al. [7] expressed the so-called "bubble growth force" for a bubble growing on a wall during pool boiling, as

$$F_{LI} = -\pi \rho_L R^2 \left[R\frac{d^2R}{dt^2} + \frac{3}{2}C_S\left(\frac{dR}{dt}\right)^2 \right] \tag{22}$$

Here, C_S is an empirical constant accounting for the presence of a wall and for the non-sphericity of the bubble. It is

taken as 20/3 in [7]. Helden et al. [8] also used Eq. (22) for studying bubble detachment in a flow along a vertical wall with C_S taken as 0.6. By using a growth law of $R = at^b$ with $b = 0.5$, a comparison of different expressions for F_{LI} is listed in Table 1.

The analytical solution given by Eq. (25) was confirmed by another theoretical analysis [39]. The coefficient in Eq. (25) (−0.29) is clearly different from that in Eq. (23) (−0.458), however, it is close to the coefficient in Eq. (24) (−0.333) for a sphere in an unbound fluid. Eqs. (26) and (27) have dramatically different coefficients (−2.25 and 0.025, respectively) which are also quite different from the coefficients in Eqs. (23)–(25). As expected from Eqs. (26) and (27), the calculation results from [8] show a negligible F_{LI}. However, from [7], F_{LI} is the only force which counteracts the buoyancy force for bubble detachment during pool boiling, based on which the departure diameters were predicted.

The comparisons of the experimental and predicted departure diameters given by Zeng et al. [7] show that, the agreement is the best for sub-atmospheric pressure with a mean deviation of 10%. For atmospheric and elevated pressures, the deviations are 15% and 26%, respectively. The big deviation for elevated pressure is a direct result of the low bubble growth rate, namely the low value of b (from 0.26 to 0.38), as noted in [7]. In fact, for this case, F_{LI} based on Eq. (22) cannot represent the overall dynamic force acting on the bubble, rather, it is smaller than the latter. As we discussed in the former sections, in case there is a necking process during bubble detachment, an additional inertia force arises in response to the accelerating rise of the bubble, and this force has no direct relationship to the bubble growth rate. This is possibly the case for bubble growth under atmospheric or elevated pressures when the bubble shows an elongated shape. Under lower pressure (higher Jakob number), the bubble growth rate can be dominantly inertia-controlled (indicated by an oblate or hemispherical bubble shape). Thus the dynamic force calculated based on the bubble growth rate is dominant, and the other effects can be neglected. Thus, the accuracy of the predicted departure diameters is actually related to the shapes of the bubbles at the detachment.

Finally, the main physics behind the predictions in [7], namely, the existence of a (single dominant resistant) force heavily depending on bubble growth rate at the moment of bubble detachment, is questionable, given the fact that, at the same time, the surface tension and the contact pressure forces were neglected based on the argument that the bubble has no connection to the wall at the moment of detachment [7]. In fact, Helden et al., [8] pointed out that the constant $C_S = (20/3)$ given by Zeng et al. [7] is too large. If Eq. (27) (with $C_S = 0.6$) were used for Zeng et al.'s predictions, the "bubble growth force" would be essentially zero.

From above, it is clear that the accurate evaluation of the liquid inertia force is very difficult in engineering practice. Rehm [11] acknowledged a big error in evaluating the liquid inertia force. In fact, different values of C_M and different expressions of u were adopted in the literature using Eq. (20) [9–12,38,40,41], some of them are without theoretical background. For calculating the drag force, " there exist various correlations for the drag coefficient and also various expressions for the bubble velocity. In [34] the drag is omitted "purposefully", based on the argument that there is no wake behind a bubble attached to a wall and therefore no drag. The error in such a force evaluation can also be caused by the inaccurate measurement of bubble geometric parameters.

In general, a big non-zero net force results from using traditional methods in evaluating various forces. In contrast, the new method presented in this paper has a clearer theoretical approach, and depends less on the experimental data. Therefore, it provides a more reliable means to evaluate the magnitude of various forces acting on a bubble which cannot be measured directly by using the measurement technologies available to date.

5. Summary and conclusions

A novel method has been developed to simulate existing bubble shapes by solving the Young–Laplace equation numerically considering the dynamic effects of bubbles growing on heating surfaces. A dynamic pressure term is added into the Young–Laplace equation which is a function of the local position of the liquid–vapor interface, and is calculated by a correlation involving several empirical coefficients. By adjusting these coefficients, a given bubble shape can be well simulated. From this simulation, the distributions of the Laplace pressure drop, the hydrostatic pressure and the dynamic pressure difference around

Table 1
Comparison of the expressions for F_{LI} using the growth law $R = at^b$ with $b = 0.5$

Ref.	F_{LI}	Eq. no.	Comments
Eq. (21)	$-0.458\pi\rho_L a^4$	(23)	$C_M = 11/16$, sphere with the presence of a plane wall
Eq. (21)	$-0.333\pi\rho_L a^4$	(24)	$C_M = 0.5$, sphere in unbound fluid
[37]	$-0.29\pi\rho_L a^4$	(25)	Analytical solution for a sphere tangent to a plane wall
[7]	$-2.25\pi\rho_L a^4$	(26)[a]	Empirical expression for bubble detachment during pool boiling
[8]	$0.025\pi\rho_L a^4$	(27)[a]	Empirical expression for bubble detachment at a vertical wall

[a] Note that the coefficients in Eqs. (26) and (27) are different from those given in [7] and [8], respectively, since the values of the exponent b (and also the coefficient a) were taken from the experimental data in these two references.

the bubble can be calculated, and the various forces acting on the bubble can also be accurately determined.

Some calculation examples have been shown for bubbles growing on smooth and enhanced heating surfaces under various conditions. The results show that, (1) a growing bubble undergoes a series of shape changes, viz. spherical, hemispherical, oblate and elongated bubbles, until the detachment stops this evolution; (2) the dynamic force greatly influences the bubble shape even for a seemingly spherical bubble (except for micro spherical bubble); (3) a pattern (shape) map of bubbles can be developed by relating the aspect ratio to the ratio of dynamic and buoyancy forces; (4) for elongated bubbles, the point where the dynamic force changes from positive to negative can serve as a criterion for bubble departure; (5) the assumption of spherical bubbles or bubble segments could lead to big errors in force evaluations in engineering practice, especially for the liquid inertia force.

The application of the developed method should not be limited to the cases studied herein. It can be used to systematically study the boiling phenomena or to verify theoretical models, A further improvement of Eq. (10) is possible and essential for simulating the bubble shapes more efficiently and more accurately.

Acknowledgement

The fellowship granted for Dr. Yuming Chen by Friedrich-Ebert-Stiftung, Germany, is greatly appreciated.

References

[1] Y. Chen, M. Groll, R. Mertz, R. Kulenovic, Visualization and mechanisms of pool boiling of propane, isobutane and their mixtures on enhanced tubes with reentrant channels, Int. J. Heat Mass Transfer 48 (2005) 2516–2528.
[2] M.S. Plesset, The dynamics of cavitation bubbles, ASME J. Appl. Mech. 16 (1949) 228–231.
[3] M.A. Johnson, J.R. Javier De La Pena, R.B. Mesler, Bubble shapes in nucleate boiling, A. I. Ch. E. J. 12 (2) (1966) 344–348.
[4] R.B.H. Tan, I.J. Harris, A model for non-spherical bubble growth at a single orifice, Chem. Eng. Sci. 41 (1986) 3175–3182.
[5] H.N. Oguz, A. Prosperetti, Dynamics of bubble growth and detachment from a needle, J. Fluid. Mech. 257 (1993) 111–114.
[6] J.F. Klausner, R. Mei, D.M. Bernhard, L.Z. Zeng, Vapor bubble departure in forced convection boiling, Int. J. Heat Mass Transfer 36 (1993) 651–662.
[7] L.Z. Zeng, J.F. Klausner, R. Mei, A unified model for the prediction of bubble detachment diameters in boiling systems—I. Pool boiling, Int. J. Heat Mass Transfer 36 (1993) 2261–2270.
[8] W.G.J.v. Helden, C.v.d. Geld, P.G.M. Boot, Forces on bubbles growing and detaching in flow along a vertical wall, Int. J. Heat Mass Transfer 38 (1995) 2075–2088.
[9] Y. Chen, M. Groll, R. Mertz, R. Kulenovic, Study of forces acting on a growing bubble from smooth and enhanced tubes, Int. J. Heat Technology 20 (2) (2002) 31–39.
[10] E.G. Keshok, R. Siegel, Forces acting on bubbles in nucleate boiling under normal and reduced gravity conditions, NASA Tech Note TND-2299, 1964.
[11] T.R. Rehm, Bubble growth parameters in saturated and subcooled nucleate boiling, Chem. Eng. Prog. Symp. Ser. 64 (1968) 88–94.
[12] N. Ginet, S. Cioulachtjian, M. Lallemand, Analysis of the forces acting on a single bubble of *n*-pentane growing on a horizontal wall, in: Proceedings of 4th International Conference on Multiphase Flow, New Orleans, USA, Paper No. 840, 2001.
[13] A. Marmur, E. Rubin, A theoretical model for bubble formation at an orifice submerged in an inviscid liquid, Chem. Eng. Sci. 31 (1976) 453–463.
[14] W.V. Pinczewski, The formation and growth of bubbles at a submerged orifice, Chem. Eng. Sci. 36 (1981) 405–411.
[15] P.E. Anagbo, J.K. Brimacombe, A.E. Wraith, Formation of ellipsoidal bubbles at a free-standing nozzle, Chem. Eng. Sci. 46 (1991) 781–788.
[16] Y. Fujita, Q. Bai, Numerical simulation of the growth for an isolated bubble in nucleate boiling, in: Proceedings of 11th International Heat Transfer Conference, Kyongju, Korea, vol. 2, pp. 437–442, 1998.
[17] G. Son, V.K. Dhir, Numerical simulation of a single bubble during partial nucleate boiling on a horizontal surface, in: Proceedings of 11th International Heat Transfer Conference, Kyongju, Korea, vol. 2, pp. 533–538, 1998.
[18] R.C. Lee, J.E. Nydahl, Numerical calculation of bubble growth in nucleate boiling from inception through departure, J. Heat Transfer 111 (1989) 474–479.
[19] J. Hammer, P. Stephan, The role of micro-region phenomena on nucleate boiling heat transfer, in: G.P. Celata et al. (Ed.), in: Proceedings of 2nd European Thermal-Science and 14th UIT National Heat Transfer Conference, pp. 467–474, 1996.
[20] A.K. Chesters, The profile and volume of a small drop or bubble, J. Fluid Mech. 81 (part 4) (1977) 609–624.
[21] S.B.G. O'Brien, On the shape of small sessile and pendant drops by singular perturbation techniques, J. Fluid Mech. 233 (1991) 519–537.
[22] B.K. Mori, W.G. Baines, Bubble departure from cavities, Int. J. Heat Mass Transfer 44 (2001) 771–783.
[23] H.K. Nahra, Y. Kamotani, Prediction of bubble diameter at detachment from a wall orifice in liquid cross-flow under reduced and normal gravity conditions, Chem. Eng. Sci. 58 (2003) 55–69.
[24] C.W.M. Van Der Geld, Bubble detachment criteria: some criticism of "Das Abreissen von Dampfblasen an festen Heizflächen", Int. J. Heat Mass Transfer 39 (1996) 653–657.
[25] Y. Chen, M. Groll, R. Mertz, R. Kulenovic, Comparison of pool boiling bubble dynamics on smooth and enhanced tubes, Int. J. Heat Technology 20 (1) (2002) 3–14.
[26] C.-Y. Han, P. Griffith, The mechanism of heat transfer in nucleate pool boiling—Part I: Bubble initiation, growth and departure, Int. J. Heat Mass Transfer 8 (1965) 887–904.
[27] S.J.D. Van Stralen, R. Cole, W.M. Sluyter, M.S. Sohal, Bubble growth rates in nucleate boiling of water at subatmospheric pressures, Int. J. Heat Mass Transfer 18 (1975) 655–669.
[28] J. Mitrovic, Formation of a liquid jet after detachment of a vapour bubble, Int. J. Heat Mass Transfer 40 (1997) 4309–4317.
[29] G.J. Jameson, A. Kupferberg, Pressure behind a bubble accelerating from rest: simple theory and applications, Chem. Eng. Sci. 22 (1967) 1053–1055.
[30] Yu.A. Buyevich, B.W. Webbon, Bubble formation at a submerged orifice in reduced gravity, Chem. Eng. Sci. 51 (1996) 4843–4857.
[31] C.v.d. Geld, Prediction of dynamic contact angle histories of a bubble growing at a wall, Int. J. Heat Fluid Flow 25 (2004) 74–80.
[32] E.E. Michaelides, Hydrodynamic force and heat/mass transfer from particles, bubbles, and drops—the Freeman Scholar lecture, J. Fluids Eng. 125 (2003) 209–238.
[33] J. Magnaudet, D. Legendre, The viscous drag force on a spherical bubble with a time-dependent radius, Phys. Fluids 10 (1998) 550–554.
[34] Yu.A. Buyevich, B.W. Webbon, Dynamics of vapour bubble in nucleate boiling, Int. J. Heat Mass Transfer 39 (1996) 2409–2426.
[35] F. Takermura, J. Magnaudet, The history force on a rapidly shrinking bubble rising at finite Reynolds number, Phys. Fluids 16 (2004) 3247–3255.
[36] C.E. Brennen, Cavitation and Bubble Dynamics, Oxford University Press, 1995.

[37] C.P. Witze, V.E. Schrock, P.L. Chambre, Flow about a growing sphere in contact with a plane surface, Int. J. Heat Mass Transfer 11 (1968) 1637–1652.

[38] Y.A. Kirichenko, Evaluation of the conditions of vapor bubble separation during nucleate boiling, J. Eng. Phys. 25 (1) (1973) 811–817.

[39] C.v.d. Geld, On the motion of a spherical bubble deforming near a plane wall, J. Eng. Math. 42 (2002) 91–118.

[40] A.P. Hatton, D.D. James, T.L. Liew, Measurement of bubble characteristics for pool boiling from single cylindrical cavities, in: Proceedings of 4th International Heat Transfer Conference, Paris, France, vol. V, B1.2, 1970.

[41] J.S. Saini, C.P. Gupta, S. Lal, Effect of Jakob number on forces controlling bubble departure in nucleate pool boiling, Int. J. Heat Mass Transfer 18 (1975) 472–474.